Materials Science and Engineering A 524 (2009) 3–9

Contents lists available at ScienceDirect

Materials Science and Engineering A

journal homepage: www.elsevier.com/locate/msea

# At the limit of polychromatic microdiffraction

Gene E. Ice[a,*], Judy W.L. Pang[a], Bennett C. Larson[a], John D. Budai[a], Jonathan Z. Tischler[a], Jae-Young Choi[b], Wenjun Liu[c], Chian Liu[c], Lahsen Assoufid[c], Deming Shu[c], Ali Khounsary[c]

[a] MST Division, Oak Ridge National Laboratory, Oak Ridge, TN 37831-6118, United States
[b] Pohang Accelerator Laboratory, Pohang, Republic of Korea
[c] Advanced Photon Source, Argonne National Laboratory, Argonne, IL 60439, United States

ARTICLE INFO

*Article history:*
Received 3 March 2009
Received in revised form 2 June 2009
Accepted 2 June 2009

*Keywords:*
Microbeam
Laue diffraction
Mesoscale
Structure
X-ray

ABSTRACT

With a high-energy 3rd generation source like the Advanced Photon Source (APS), it is possible to push the performance of polychromatic microdiffraction far beyond current levels and to approach the intrinsic limit of the technique based on sample damage and the diffraction limit of X-rays. We describe ongoing efforts to improve the spatial, temporal and momentum transfer resolution of polychromatic microdiffraction on beamline 34-ID-E at the APS. The goal of this effort is to provide high-resolution images of 3D crystal structures over sufficient volumes and with sufficient detail to clarify the underlying physics of inhomogeneous structure and evolution on mesoscopic length scales. The performance of a high-speed amorphous Si area detector system and the ongoing development of advanced focusing optics will be described and discussed in light of the ultimate limits set by the physics of X-rays and materials, and in light of opportunities to field specialized insertion devices and optics for polychromatic microdiffraction.
© 2009 Elsevier B.V. All rights reserved.

## 1. Introduction

Polychromatic microdiffraction is a powerful probe of local crystal structure made possible by ultra-brilliant X-ray sources, efficient area detectors and high-performance X-ray focusing optics [1–3]. Beamlines using this approach are now in place at the Advanced Light Source [4], Swiss Light Source [5], National Synchrotron Light Source [6], Pohang Light Source [7], Canadian Light Source [8] and Advanced Photon Source (APS) [3]. Other beamlines are planned for the Australian Light Source [9], SOLEIL [10] and elsewhere. With the basic technique, submicron X-ray beams with a broad energy spectrum are used to probe small sample volumes (Fig. 1). With depth resolution, focused X-ray microbeams resolve heterogeneous samples into near-homogeneous volumes for which the polychromatic diffraction pattern determines the local crystallographic orientation, and the local elastic and plastic deformation [11]. Spatial resolution along the probing beam direction can be achieved by the use of differential aperture microscopy (Fig. 1), which allows for true 3D submicron spatial resolution [12]. Currently only station 34-ID-E at the APS has reported complete 3D capability with differential aperture microscopy.

The special requirements of polychromatic microdiffraction have led to the development of unique instrumentation including non-dispersive X-ray microfocusing optics [13–16], high-performance non-dispersive monochromators with absolute wavelength calibration [17,18], a profiling wire technique [11], and a specialized software [19–21]. In addition, specialized high-performance X-ray detectors and dedicated data analysis hardware extend the range of experiments that can be contemplated [22].

Because beamline 34-ID-E is on a high-energy 3rd generation undulator source with ~2 orders of magnitude higher integrated brilliance than other polychromatic microbeam sources [22], and because it is the only polychromatic probe with differential aperture microscopy, it serves as a test bed for new techniques, and offers insights into the ultimate capabilities that will be possible with the next generation of X-ray sources. Indeed, the suite of novel instrumentation on beamline 34-ID-E allows for a range of experimental techniques that would be difficult on other instruments and which promise even more advanced techniques in the future. These include: (1) differential aperture microscopy (wire scan) studies to determine 3D spatially resolved maps of the local elastic deviatoric strain, crystallographic orientation and unpaired dislocation density and (2) combined energy/wire scans to measure the absolute local strain tensor [23].

Although polychromatic microdiffraction is a very powerful tool for nondestructive investigation of the evolution of mesoscale structures, the technique is inherently a scanning point-probe method that (as all scanning techniques) is relatively slow when

* Corresponding author at: MST Division, Oak Ridge National Laboratory, Rm B256, Bldg 4500S, ORNL, 1 Bethel Valley Road, Oak Ridge, TN 37831-6118, United States. Tel.: +1 865 574 2744; fax: +1 865 574 7659.
*E-mail address:* IceGE@ornl.gov (G.E. Ice).

0921-5093/$ – see front matter © 2009 Elsevier B.V. All rights reserved.
doi:10.1016/j.msea.2009.06.001

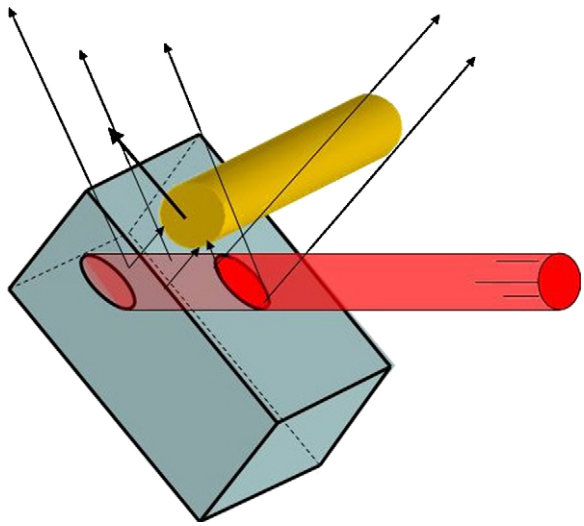

**Fig. 1.** A probing microbeam resolves submicron regions of the sample. Resolution along the beam is achieved using a profiling wire that scans through the diffraction pattern close to the sample. The wire shadow projected onto the detector is analyzed by triangulation to calculate the Laue pattern generated by submicron volumes along the beam.

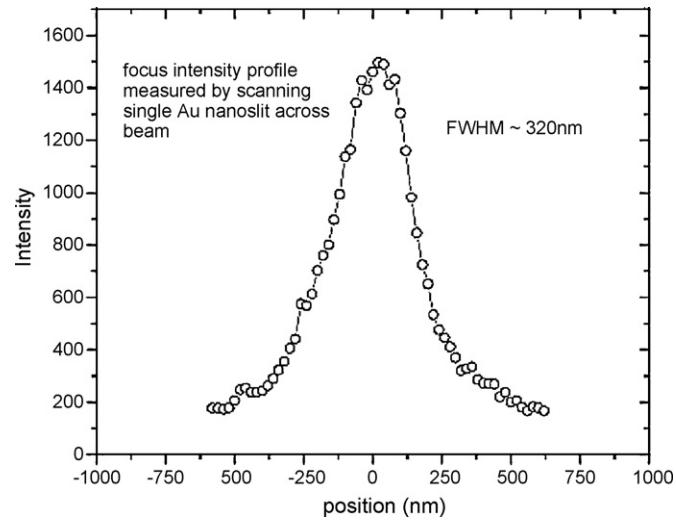


**Fig. 3.** Typical focal spot size on 34-ID-E with Pt-coated microfocusing mirrors. The mirror surfaces were deposited on flat Si substrates. The mirror performance was stable for ~6 months of normal operations but degraded after continuous exposure to the direct beam required for continuous data acquisition with a faster detector.

significant volumes are analyzed. This problem can be reduced by fielding faster detectors and by the use of specialized insertion devices and new sources. Indeed, upgrades to the current APS have the potential to deliver an order of magnitude more intense beam (Fig. 2), and 4th generation sources offer even higher performance opportunities.

Below we describe the status of new instrumentation on beamline 34-ID-E and the implications for experimental measurements in the near future. We further speculate on the ultimate performance that will arise from the use of polychromatic microprobe ideas on 4th generation synchrotron sources including issues of coherence, temporal resolution and damage.

## 2. Spatial resolution

The smaller the focused beam spot size, the smaller the volume probed and the higher the achievable resolution in all three dimensions. Beamline 34-ID-E uses differentially profiled X-ray mirrors [13–15] to focus the beam to an ~300 nm size (Fig. 3). This approach has demonstrated beams as small as ~80 nm [14], and the ultimate spatial resolution of non-dispersive mirror focusing optics as set by the diffraction limit of total-external-reflection mirrors is ~17 nm [16]. Yamauchi et al. have demonstrated doubly focused beams of ~24 nm from diffraction-limited total-external-reflection KB optics [24] and singly focused beams from multilayers below 14 nm [25]. However, for a useable polychromatic microdiffraction device to approach this level of spatial resolution routinely, positional stability must be maintained at the nm level between the sample and the focusing optics and at submicroradian angular level between the focusing optics and the beamline axis (Fig. 3). Challenges include mirror figure stability, thermal drifts of components and vibration contributions to misalignment. With existing instrumentation nanometer stability is hard to maintain – although experience at the nanoprobe beamline X25 of the APS is encouraging [26].

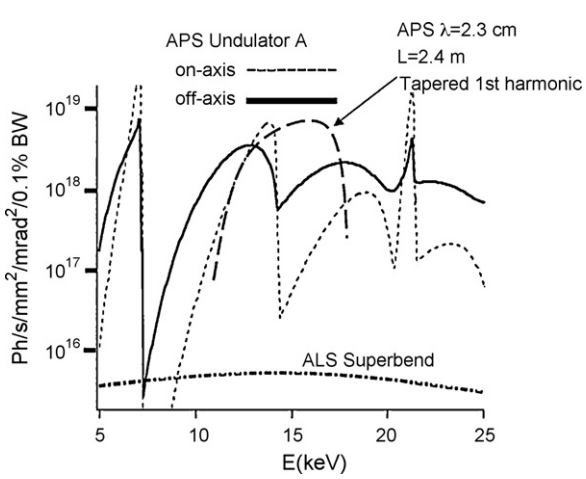


**Fig. 2.** (a) Brilliance of an undulator A on axis; (b) brilliance of undulator APS undulator A off axis; (c) brilliance of ALS superbend; (d) brilliance of optimized upgrade undulator on APS.

Over the last year, there have been two research efforts on 34-ID-E optics aimed at improving long-term and short-term beam stability. One effort has been directed toward making the mirror surfaces stable on at least a yearly time scale. The other effort has been directed at minaturizing the mirror mounts and simplifying the degrees of freedom to improve vibration and thermal stability. Consider for example recent efforts lead by Chian Liu at Argonne to develop more stable profile coated mirrors [27]. A guiding principle on 34-ID-E has been the use of prefigured mirrors to eliminate the complexity of dynamical bending systems and to provide for more stable operations; prefigured mirrors including differentially profiled mirrors should be inherently more stable than bent mirrors because they can be lighter and because they are not as sensitive to thermal gradients. However, with profiled mirrors, damage to the mirrors during use and aging of the mirrors due to relaxation of residual strains can limit the long-term stability of the reflecting surfaces. We have observed serious local degradation of Au profiled surfaces when the mirrors are exposed to intense un-apertured beams. Similarly we have observed global changes in Au profiled surfaces with time; mirrors with initially small surface figure errors have been observed to deteriorate during use and even when on the shelf. Major progress has been made recently to correct these issues. This progress is reported in Ref. [27] and is based on the use of stiffer (thicker) substrates, thinner coatings and Pt for profiling. Mirrors coated with Pt showed no deterioration of their focusing properties after ~6 months of continuous operation. However, recent exposure to continuous white beams has resulted in possible surface deterio-

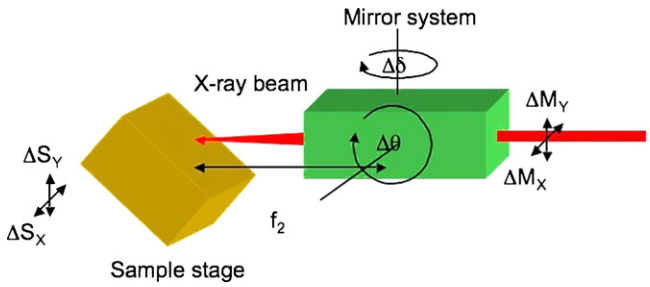


**Fig. 4.** Beam stability requires good registration between the sample stage and the focusing optical stage. Both gradual long-term drifts and transient displacement are undesirable. With mirror optics the focal spot position is sensitive to very small angular errors.

ration. Further efforts to use thinner profile coatings on pre-shaped surfaces are continuing.

On the short-term time scale mirror resolution is limited by vibration of the sample and optical mount (Fig. 4) and by thermal drifts of the components. In addition to the use of a massive optical table, and a layered approach to temperature control, an emerging strategy for improving beam stability on the sample is through a simplified alignment geometry that minimizes the degrees of freedom at the sample. Consider for example the design of Fig. 5A where two mirrors are aligned optically prior to use. With this so-called Montel geometry, the key alignment step is to make the mirror surfaces perpendicular. This can be done by reflecting a laser beam off the corner between the two mirrors. The beams reflecting in opposite mirror order interfere and create a diffraction pattern that can be easily adjusted to 100 μrad. This orthogonality is sufficient to focus a 100 μm beam to 10 nm. The beam can be centered on the two mirrors either by the upstream adjustment of an over-illuminated slit, or by actually adjusting the electron beam axis to center it on the surveyed mirror assembly. With this approach, only two rotational degrees of freedom are included in the mirror assembly with the stage accurately mounted with precision-machined parts to the beam axis. Although this approach requires careful pre-alignment, at least two translation stages are eliminated. This approach reduces the complexity of the mirror stage and should allow for a more robust instrument; in addition, because the system is pre-aligned prior to use, only small angular adjustments are needed at the mirror stage (Fig. 5B). A picture of a prototype mirror assembly is shown in Fig. 6. We note that the Montel geometry requires the use of the edge of at least one mirror. This is a technical challenge since prepolished mirrors typically have roundoff errors at the edges. However, recent experience has shown that small mirrors can be cut from larger polished substrates with negligible change in the local figure. This should allow for the fabrication of precision mirrors with good figure and roughness near their edges.

## 3. Data collection speed

On 34-ID-E, Laue images of annealed grains in polycrystalline materials take ~1–20 ms of exposure, and images of highly deformed materials typically take ~100–500 ms of exposure. Unfortunately, the readout speed of the 34-ID-E CCD has been ~2–6 s depending on compromises made in number of pixels recorded. This has resulted in a data collection to sample exposure ratio of between 4 and 6000. We have now installed a detector system based on tiled amorphous Si detectors. This system will provide much faster ultimate readout capabilities of 12–15 fps with 6 megapixels and 25–30 fps with 1.5 megapixels (binned 2 × 2). In addition to high readout speed, initial tests indicate that the detector exhibits much lower tails in the point-spread-function, much reduced blooming and has much better absolute positioning of the pixels for more accurate strain tensor measurements. For example, the measured angular positions of Laue spots is at least four times more accurate than with a previous CCD with 1:1 fiber optical coupling between the CCD and the phosphor screen. This gives confidence that elastic strains can be measured to $<5 \times 10^{-5}$ in cases where deformation is not extreme.

The detector framework with two of the three amorphous Si modules in place is shown in Fig. 7. Initial tests are underway to collect data in a standard step scan mode at up to 4 fps. However, step scanning is impractical for faster data collection due to the settling time of the sample stage. As a result, slew scanning or "on

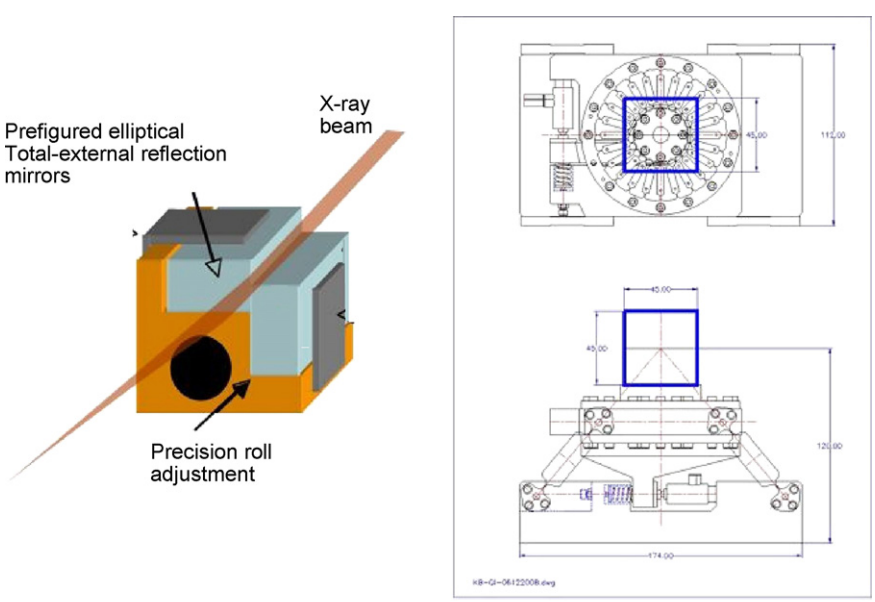


**Fig. 5.** (A) Nested mirrors are pre-aligned on a compact fixture using laser interference to precisely set the relative roll, and with force or microscope alignment of the spacing between the mirrors. (B) The precision tilt stages require only a very small angular range due to pre-alignment of the optics. This should allow for an ultra-stable mirror focusing system.

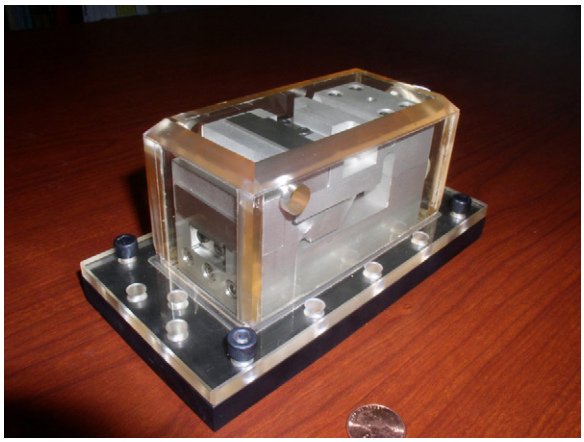

**Fig. 6.** Prototype mirror assembly for nested mirror pair. All adjustments are manual except for the mirror tilts.

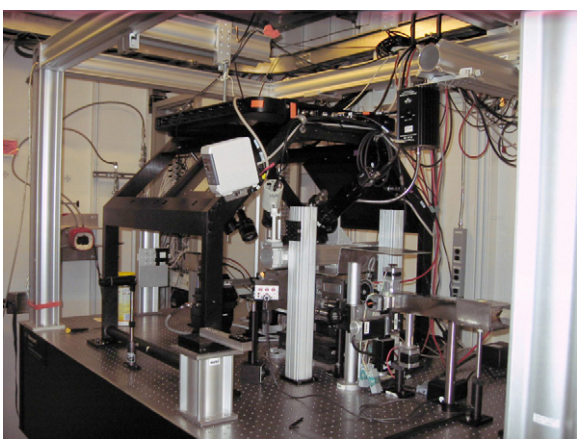

**Fig. 7.** Newly installed area detector system with large format amorphous Si detectors.

the fly scanning" is planned to approach the 15–30 fps readout limit of the detector.

Of course the amorphous Si detector has drawbacks for certain experiments. Because it is not cooled, it has slightly higher noise than a CCD and cannot collect data for long periods of time without multiple readout cycles. In addition the large pixel size complicates differential aperture microscopy and requires the use of larger wires to cut the beam. These complications are however acceptable due to the much more efficient use of precious synchrotron radiation beamtime (less wasted time in readout) and the ability to map more volume elements with better strain resolution.

## 4. Sample damage

Damage is an important ultimate limit that depends critically on the nature of the sample, the total dose, the dose rate and the beam wavelength. Intrinsically X-rays are the most sensitive non-destructive probe of high Z trace elements in low Z substrates [28]. However, the large photoelectric cross-section/elastic scattering cross-section of X-rays makes them more damaging than electrons and much more damage than neutrons for the same structural information. As a consequence, the ultimate limit for X-ray structural measurements for small samples is thought to be somewhat less than for electron probes. However X-rays have a unique combination of source brilliance and penetrating power that makes them indispensable for structural studies of small subsurface, layered and/or 3D objects. There are a number of strategies aimed

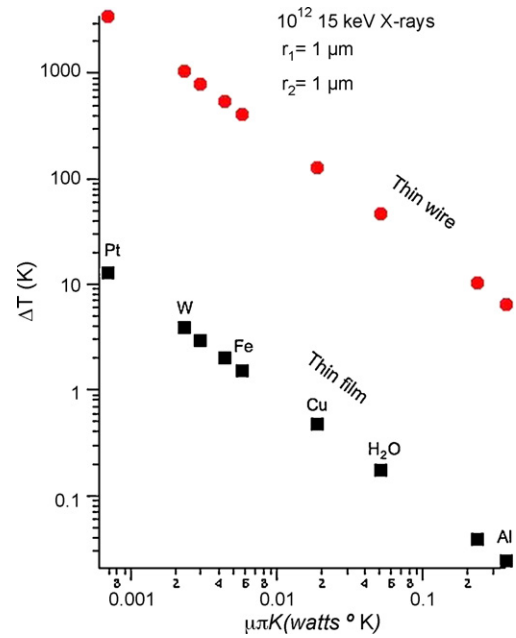


**Fig. 8.** Estimated thermal rise for an ~1 μm X-ray beam with $10^{12}$ 15 keV photons incident on either a thin wire or a thin film. The sample is cooled with a thermal sink approximately 0.5 mm from the beam.

at reducing damage. These include cryo-cooling, measurements on small sample volumes, and flash measurements. Unfortunately these approaches are in general not consistent with in situ nondestructive monitoring of mesoscale structural evolution.

Although there is a rich literature regarding damage in biological samples, there is much less information on damage in oxides and metals. In general, biological samples are found to damage under even monochromatic beam measurements [29], although measured temperature rises with monochromatic synchrotron illumination are found to be small [30].

Nevertheless, estimates of polychromatic microbeam damage have focused on thermal evolution in materials with the assumption that structural materials are fundamentally radiation resistant to X-radiation. The concern is that thermal excursions and thermal gradients can deform or even melt the local structure. After all it is well known that undulator beams from 3rd generation synchrotrons can deliver higher thermal densities than the surface of the sun. There is therefore considerable concern about thermal excursions with focused polychromatic irradiation.

To illustrate the thermal behavior of various kinds of samples we consider the response of thin film samples and wire samples to a penetrating X-ray beam. The thin film sample can also serve as a conservative approximation to the near-surface behavior of a small penetrating beam into a bulk sample. The thermal rise in a thin film can be estimated analytically by assuming that the total beam power $P_0$ is uniformly distributed in a circular cross-section of radius, $r_1$, and is cooled by a massive heat sink at radius $r_2$. In this approximation, the temperature rise $\Delta T$ depends primarily on the total power in the beam, and the sample linear absorption coefficient, $\mu$, and thermal conductivity, $K$, so that:

$$\Delta T = \frac{P_0}{2\pi\mu K}\left(\frac{1}{2} + \ln\left(\frac{r_1}{r_2}\right)\right) \quad (1)$$

From Eq. (1) it is clear that for thin films, the thermal rise is mainly dependent on the material and the total power and is relatively insensitive to the beam size or heat sink geometry. Similarly we can estimate the thermal rise in a small wire illuminated by a beam of cross-section $r_1$ and cooled by a massive thermal sink at a distance

$\pm r_2$ from the beam center:

$$\Delta T \approx \frac{P_0}{\pi \mu K}\left(\frac{r_2}{r_1} - \frac{1}{2}\right). \quad (2)$$

Here the thermal rise is *linear* with $r_2$ so that a long wire with say a 1000× longer distance to the heat sink than the size of the beam will experience a much larger thermal rise than a similar thin film for which the heat flow is radial and two-dimensional. The thermal rise is also inversely proportional to the wire radius. Anticipated temperature rises for realistic conditions are considered in Fig. 8. We note that these curves can be scaled to total power to predict the behavior of new high-performance synchrotron sources.

Of course thermal excursions are only a consideration for very radiation-hard materials. Indeed lattice-displacement damage or bond breaking is observed more often than reported because experiments compromised by the damage either are modified to avoid damage or discontinued. For example, Ice, McKee and co-workers studied the ferroelectric polarization in $BaTiO_3$ film plateaus with a monochromatic microbeam circa 1996 in which they found major electrical property changes in the irradiated plateaus [31]. Recently, Cargill [32] has found electrical property changes in metal interconnects after exposure to polychromatic microbeams. These changes were attributed to defect creation in the passivation layers around the interconnects. Specht attempted structural microbeam measurements on surrogate explosive materials but found that they decomposed under polychromatic microbeam irradiation [33]. More recently Noyan and co-workers has observed radiation damage in monochromatic nanobeam irradiated materials [34]. Figs. 9 and 10 show optical photomicrographs and Laue diffraction patterns respectively from EuAlO nanobelts which exhibit changes in local optical properties and lattice perfection due to radiation damage.

## 5. Implications of polychromatic instrumentation for coherence imaging

Laue diffraction records radial line integrals through reciprocal space. These line integrals can be differentiated along the radial direction by inserting a monochromator and then scanning the X-ray energy. As is well known, for very small objects, the focused X-ray beams from a polychromatic probe will scatter coherently for every wavelength in the beam. As illustrated below, under some symmetry conditions even polychromatic diffraction can show interference effects and consequently polychromatic methods hold promise for advanced coherent diffraction analysis of ultra-small objects. In all cases, scattering from very small particles will exhibit diffraction broadening that must be deconvoluted from other contributions to spot size and shape. A major advantage of Laue diffraction is the simultaneous scattering into distinct angular directions for crystalline particles of different orientations and the assurance that Bragg reflections (Laue spots) will be detected independent of the particle orientation.

For simplicity we consider an ideal cubic particle with a simple cubic Bragg lattice as illustrated in Fig. 11. If the real-space lattice vector is $a_0$, the reciprocal space lattice vector is $1/a_0$ and at a reciprocal lattice point the density distribution will be proportional to:

$$I \propto \frac{\sin^2 Nx}{\sin^2 x}\frac{\sin^2 Ny}{\sin^2 y}\frac{\sin^2 Nz}{\sin^2 z}. \quad (3)$$

Here $N$ is the number of atoms along each side of the cubic particle. The Laue pattern generated near each Laue spot is a projection of the Fourier transform of the real-space particle. The projection direction depends on the momentum transfer of the individual Bragg reflection. For example, if the radial direction is along a symmetry direction (say the $z$ direction) then the $z$ dependence is removed and the Laue spot contains only information about the transverse particle size (see Fig. 11). Of course energy scans through the reflection provide information about the local coherent reciprocal space density distribution.

Fig. 12A illustrates the calculated diffraction near the center of the 34-ID-E area detector with a monochromatic, $\lambda = 0.14$ nm, beam and a hypothetical 15 nm particle with a perfect simple cubic lattice with $a_0 = 0.3$ nm. The modeled pixel size of 0.4 mm is actually twice that of the actual detector on 34-ID-E. Even so, as can be seen, the pattern is easily resolved by the detector and even larger particles should be amendable to coherent imaging with the current system. We note that a 200 eV bandpass (∼3%) as illustrated in Fig. 12A looks very similar to a monochromatic image. Even at 1 keV bandpass (11%) the image shows marked coherent structure, in part because the radial integrals are parallel to a symmetry direction.

Polychromatic microdiffraction instrumentation naturally lends itself to such measurements. The small beams produced by the focusing optics increase the flux density at the sample at the expense of transverse coherence [35,36]. This is important for detection of the smallest features, which are inherently weak scatterers. The non-dispersive energy scanning methods pioneered for polychromatic microdiffraction also allow the volume of reciprocal space near the Laue spot to be probed to determine the 3D density profile of the Laue spot without the complication of

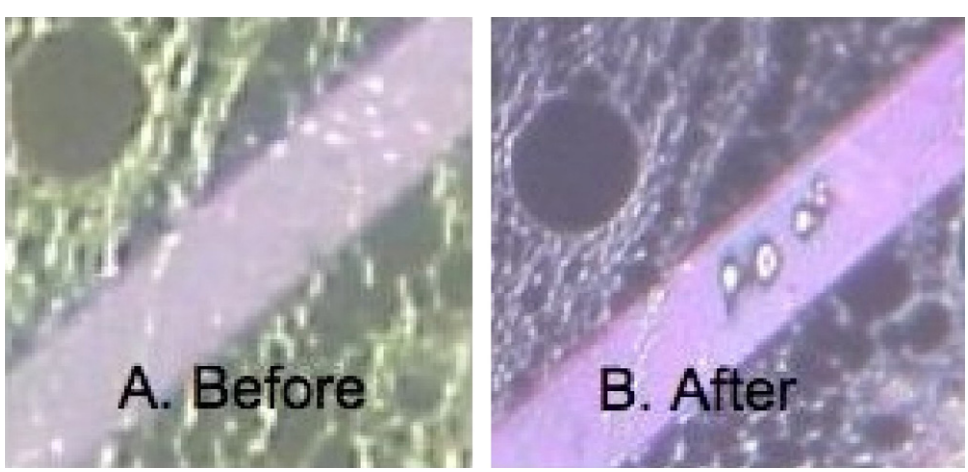


**Fig. 9.** Optical photomicrographs showing an ∼6 μm wide EuAlO nanobelt (A) before and (B) after irradiation. Beam damage is observed where beam was positioned for several minutes.

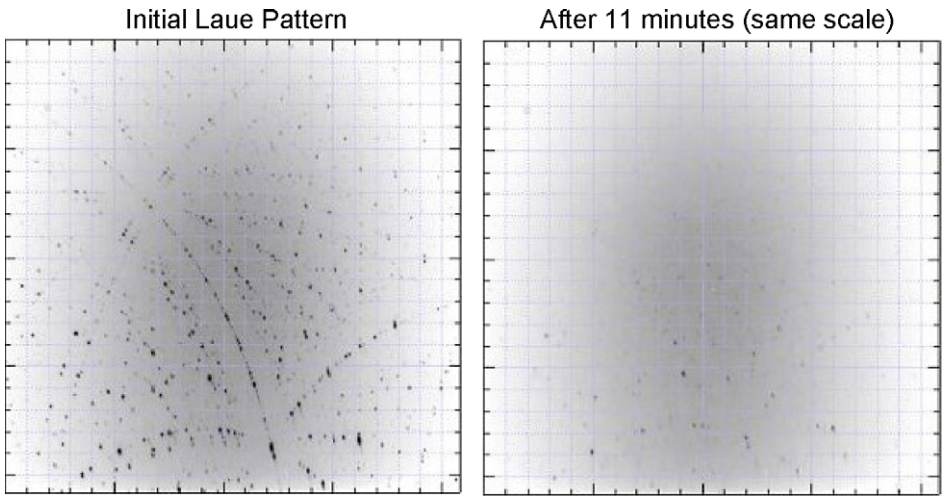


**Fig. 10.** Laue image degradation with dose in oxide nanobelts indicates lattice damage.

sample rotations. Furthermore, additional Bragg reflections can be probed. These additional projections through reciprocal space can be important to remove artifacts that may be introduced by the coherent scattering of the focusing and monochromatizing optics [32].

The current size limit to a detectable particle can be estimated from a recent paper by Schroer et al. [35]. In a transmission geometry, with focused 100 nm × 100 nm beam, a total integrated flux of ~$6 \times 10^{10}$ photons was sufficient to image spheres with ~5 nm resolution. These numbers predict near atomic resolution with a flux of $2 \times 10^{14}$ photons in a 10 nm × 10 nm beam. Achromatic optics are the most likely to achieve this flux density in the near term. At the LCLS, photon fluxes of $10^8$–$10^{12}$ are predicted/pulse. At the proposed Cornell hard-energy ERL, it is projected that photon fluxes of 1–8 × $10^{14}$ $s^{-1}$ will be possible into 10 nm × 10 nm spots. With wide bandpass these flux densities may be achieved earlier – although the longitudinal coherence length will be proportionally shortened.

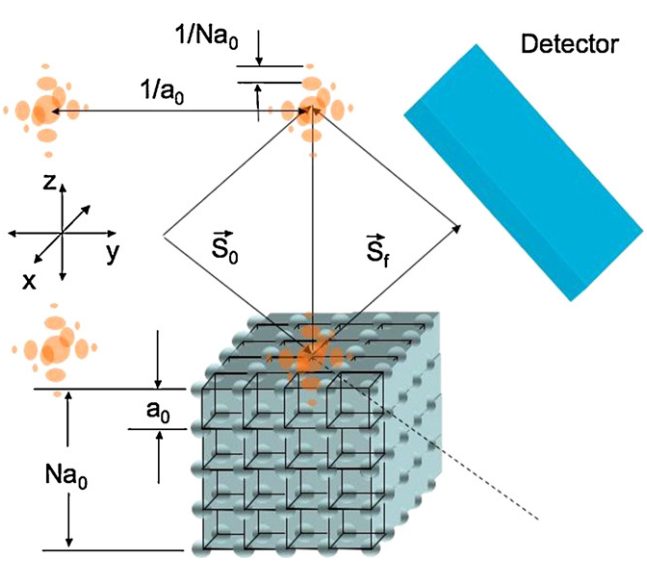


**Fig. 11.** A simple real-space lattice with a graphical representation of the corresponding reciprocal space lattice. Coherence features will be observed even with polychromatic beams if the radial line integrals are symmetric with respect to a symmetry axis of the particle. Of course atomic resolution is beyond current resolution, but features of broadening and constructive and destructive interference are anticipated under the right conditions.

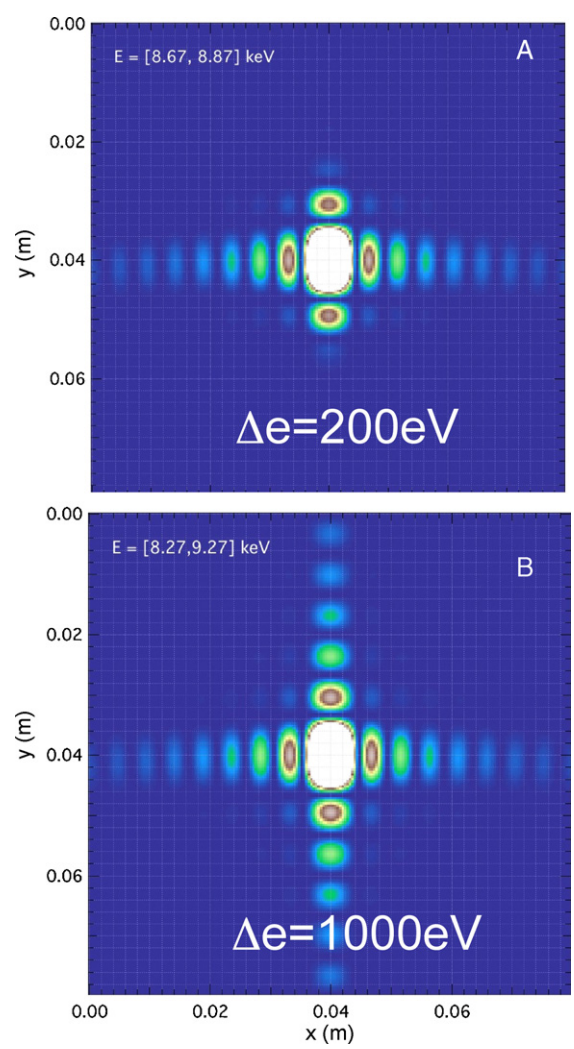


**Fig. 12.** (A) 3% bandpass diffraction pattern for an ultra-small 15 nm cubic particle. The mirror symmetry arises from the angle of the Ewald sphere cut through reciprocal space. (B) Because the radial integrals run parallel to one of the particles symmetry axis, even a 11% bandpass beam shows strong coherent structure.

## 6. Conclusion

Polychromatic microdiffraction can be pushed to new levels of performance with better detectors and sources. Faster detectors and more brilliant sources will allow for diffraction tomography over larger volumes with better spatial resolution. However, for some materials, thermal effects and damage are already an issue and new strategies will be required to extend spatial resolution or follow mesoscale structural evolution in these systems. For many materials, damage is not yet an issue and both spatial resolution and temporal resolution can be improved. The longitudinal spatial resolution achievable with a straightforward extension of scanning probe methods is limited by the spot size for which total-external-reflection mirrors is limited to ∼11–17 nm. Coherent diffraction offers the promise of further improving spatial resolution and by combining instrumentation and techniques from polychromatic diffraction, with software and methods from diffraction imaging there is the potential to reveal local structures and defects that are difficult to characterize with alternative techniques.

## Acknowledgements

G.E.I., J.W.L.P., B.C.L., J.D.B. and J.Z.T. sponsored by the Division of Materials Sciences and Engineering, U.S. Department of Energy, under Contract DE-AC05-00OR22725 with UT-Battelle LLC. Research in part at the APS which in addition to W.L., D.S. and A.K. is supported by the U.S. Department of Energy, Office of Science, Office of Basic Energy Sciences, under Contract No. DE-AC02-06CH11357. This submission has been authored in part by scientists under contract to the Department of Energy. The U.S. Government retains a nonexclusive, license to publish or reproduce this submission.

## References

[1] G.E. Ice, B.C. Larson, Adv. Eng. Mater. 2 (2000) 643–646.
[2] W.J. Liu, G.E. Ice, B.C. Larson, W.G. Yang, J.Z. Tischler, J.D. Budai, Metall. Mater. Trans. A 35 (2004) 1963–1967.
[3] G.E. Ice, B.C. Larson, MRS Bull. 29 (2004) 170–176.
[4] M. Kunz, N. Tamura, K. Chen, A.A. MacDowell, R.S. Celestre, M.M. Church, S. Fakra, E.E. Domning, J.M. Glossinger, J.L. Kirschman, G.Y. Morrison, D.W. Plate, B.V. Smith, T. Warwick, V.V. Yashchuk, H.A. Padmore, E. Ustundag, Rev. Sci. Instrum. 80 (2009) 035108.
[5] R. Maass, S. Van Petegem, H. Van Swygenhoven, P.M. Deriet, C.A. Volkert, D. Grolimund, Phys. Rev. Lett. 99 (2007) 145505.
[6] K. Evans-Lutterodt, Private communication (2008).
[7] J.H. Park, J. Park, K.B. Lee, T.Y. Koo, H.S. Youn, Y.D. Ko, J.S. Chung, J.Y. Hwang, S.Y. Jeong, Appl. Phys. Lett. 91 (2007) 012906.
[8] R. Feng, A. Gerson, G. Ice, R. Reininger, B. Yates, S. McIntyre, in: J.-Y. Choi, S. Rah (Eds.), Synchrotron Radiation Instrumentation: Ninth International Conference, vol. 879, American Institute of Physics, 2007, pp. 872–874.
[9] http://www.unisa.edu.au/synchrotron/Microdiffraction_beamline/Default.asp.
[10] http://www.synchrotron-soleil.fr/images/File/soleil/ToutesActualites/Archives-Workshops/2007/SUM07/22-SUM07-GOUDEAUPhilippe1.pdf.
[11] G.E. Ice, R.I. Barabash, J.W.L. Pang, Encyclopedia of Materials: Science and Technology Updates, Elsevier, Oxford, 2005.
[12] B.C. Larson, W. Yang, G.E. Ice, J.D. Budai, J.Z. Tischler, Nature 415 (2002) 887–890.
[13] G.E. Ice, J.-S. Chung, J.Z. Tischler, A. Lunt, L. Assoufid, Rev. Sci. Instrum. 71 (2000) 2635–2639.
[14] W. Liu, G.E. Ice, J.Z. Tischler, A. Khounsary, C. Liu, L. Assoufid, A.T. Macrander, Rev. Sci. Instrum. 76 (2005), 113701/1.
[15] C. Liu, L. Assoufid, R. Conley, A.T. Macrander, G.E. Ice, J.Z. Tischler, Opt. Eng. 42 (2003) 3622–3628.
[16] G.E. Ice, Nucl. Inst. Meth. 582 (2007) 129–131.
[17] G.E. Ice, J.-S. Chung, W. Lowe, E. Williams, J. Edelman, Rev. Sci. Instrum. 71 (2000) 2001–2006.
[18] N. Tamura, A.A. Macdowell, R. Spolenak, B.C. Valek, J.C. Bravman, W.L. Brown, R.S. Celestre, H.A. Padmore, B.W. Batterman, J.R. Patel, J. Synchr. Rad. 10 (2003) 137–143.
[19] J.S. Chung, G.E. Ice, J. Appl. Phys. 86 (1999) 5249–5256.
[20] N. Tamura, A.A. MacDowell, R.S. Celestre, H.A. Padmore, B. Valek, J.C. Bravman, R. Spolenak, W.L. Brown, T. Marieb, H. Fujimoto, B.W. Batterman, J.R. Patel, Appl. Phys. Lett. 80 (2002) 3724–3727.
[21] V.K. Gupta, S.R. Agnew, J. Appl. Crystallogr. 42 (2009) 116–124.
[22] G.E. Ice, Metall. Mater. Trans. A 39A (2008) 3058–3064.
[23] W.G. Yang, B.C. Larson, G.E. Ice, J.Z. Tischler, J.D. Budai, K.S. Chung, W.P. Lowe, Appl. Phys. Lett. 82 (2003) 3856–3858.
[24] H. Mimura, H. Yumoto, S. Matsuyama, Y. Sano, K. Yamamura, Y. Mor, M. Ybashi, Y. Nishino, K. Tamasaku, T. Ishikawa, K. Yamuchi, Appl. Phys. Lett. 90 (2007) 051903.
[25] Yamauchi, Private communication (August 2008).
[26] H.F. Yan, O. Kalenci, I.C. Noyan, J. Maser, J. Appl. Crystallogr. 104 (2008) 023506.
[27] C. Liu, R. Conley, J. Qian, C.M. Kewish, W. Liu, L. Assoufid, A.T. Macrander, G.E. Ice, J.Z. Tischler, Nucl. Inst. Meth. A (2008), in press.
[28] C.J. Sparks, in: H. Winick, S. Doniach (Eds.), Synchrotron Radiation Research, Plenum Press, New York, 1980.
[29] J.M. Holton, J. Synchr. Rad. 16 (2009).
[30] E.H. Snell, H.D. Bellamy, G. Rosenbaum, M.J. van der Woerd, J. Synchr. Rad. 14 (2007) 109–115.
[31] R.A. McKee, F.J. Walker, G.E. Ice, Unpublished measurements (1996).
[32] Cargille, Private communication (2008).
[33] E.D. Specht, Private communication (2008).
[34] S.M. Polvino, C.E. Murray, O. Kalenci, I.C. Noyan, B. Lai, Z.G. Cai, Appl. Phys. Lett. 92 (2008) 22415.
[35] C.G. Schroer, R. Boye, J.M. Feldkamp, J. Patommel, A. Schroop, A. Schwab, S. Stephan, M. Burghammer, S. Schoder, C. Riekel, Phys. Rev. Lett. 101 (2008) 090801.
[36] C. Rau, V. Crecea, C.P. Richter, K.M. Peterson, P.R. Jemian, U. Neuhausier, G. Schneider, X. Yu, V. Braun, T.C. Chiang, I.K. Robinson, Micro Nano Lett. 2 (2007) 1–5.